Applied Radiation and Isotopes 83 (2014) 77–85

Contents lists available at ScienceDirect

Applied Radiation and Isotopes

journal homepage: www.elsevier.com/locate/apradiso

Low-energy electron and positron transport in gases and soft-condensed systems of biological relevance

R.D. White [a,*], W. Tattersall [a], G. Boyle [a], R.E. Robson [a], S. Dujko [b], Z.Lj. Petrovic [b], A. Bankovic [b], M.J. Brunger [c,d], J.P. Sullivan [e], S.J. Buckman [e,d], G. Garcia [f]

[a] ARC Centre for Antimatter–Matter Studies, School of Engineering and Physical Sciences, James Cook University, Townsville 4810, Australia
[b] Institute of Physics, University of Belgrade, P.O. Box 68, Pregrevica 118, 11080 Zemun, Belgrade, Serbia
[c] ARC Centre for Antimatter–Matter Studies, School of Chemical and Physical Sciences, Flinders University, GPO Box 2100, Adelaide, SA 5001, Australia
[d] Institute of Mathematical Sciences, University of Malaya, 5063 Kuala Lumpur, Malaysia
[e] ARC Centre for Antimatter–Matter Studies, Research School of Physical Sciences, Australian National University, Canberra, ACT, Australia
[f] Instituto de Física Fundamental, Consejo Superior de Investigaciones Científicas, Madrid 28006, Spain

HIGHLIGHTS

- Detail differences in electron/positron transport in water in gas and liquid states.
- Emphasizes the importance of swarms as a test of accuracy/completeness of cross-sections.
- Emphasizes the importance of swarms for benchmarking Monte-Carlo simulations.
- Demonstrates the sensitivity of low-energy positron thermalization to cross-sections.

ARTICLE INFO

Available online 11 January 2013

Keywords:
Positron transport
Cross sections
Radiation damage modeling
Monte-Carlo simulation
Swarm physics

ABSTRACT

We present a study of electron and positron transport in water in both the gaseous and liquid states using a Boltzmann equation analysis and a Monte-Carlo simulation technique. We assess the importance of coherent scattering processes when considering transport of electrons/positrons in dense gases and liquids. We highlight the importance of electron and positron swarm studies and experiments as a test of the accuracy and completeness of cross-sections, as well as a technique for benchmarking Monte-Carlo simulations. The thermalization of low-energy positrons (<150 eV) in water is discussed and the sensitivity of the profiles to the form of the cross-sections in this energy region, and assumptions in the microscopic processes, is considered.

1. Introduction

The study of electron and positron transport in biological matter is a key area of research in a variety of medical fields. Positrons, the antiparticle of the electron, are now a routinely used tool in imaging technologies such as positron emission tomography (PET) (Cherry et al., 2003) and in new therapeutic treatments such as positherapy and ion-beam therapy. In the latter, nuclear fragmentation of incident ions can often generate positron emitting particles, which can then provide a measure of the dose depth distribution for the ion beams (Enghardt et al., 2004). Positrons are emitted typically at hundreds of keV and must thermalize in human tissue down to a few hundred eV or less, before they can form positronium (Ps) or annihilate directly. The observation of the emitted back-to-back gamma rays arising from the annihilation is the key physics associated with these tools. Consequently, the source of the gamma rays is displaced from the source of positrons. Understanding the positron thermalization process is essential to optimizing the technologies and informing the development of positron dosimetry models. There is also a second issue of ionizing radiation involved in many imaging and therapeutic technologies, which by definition liberates copious numbers of secondary electrons along its path. Typically these electrons are produced with energy distributions less than 20–30 eV. These low-energy electrons thermalize in human tissue through a variety of energy deposition processes. Although low in energy, these electrons have recently been shown to be a source of DNA damage (Boudaiffa et al., 2000) and hence understanding the transport of low-energy

* Corresponding author. Tel.: +61 747814197.
E-mail address: ronald.white@jcu.edu.au (R.D. White).

0969-8043/$ - see front matter © 2013 Elsevier Ltd. All rights reserved.
http://dx.doi.org/10.1016/j.apradiso.2013.01.008

secondary electrons is key to understanding radiation damage and informing dosimetry models.

Water is often used as a surrogate for modeling human tissue. Modeling charged particle transport in human tissue is dependent on, amongst other things (i) an accurate microscopic picture involving a complete and accurate set of cross-sections for positrons and electrons in water, and (ii) an accurate transport theory/simulation linking the microscopic and macroscopic scales. This is the focus of our program and the current paper.

Compilation of the best available set of cross-sections for all collisional processes (e.g. elastic, rotations, vibrations, etc.) is generally based on a critical assessment of available experimental studies and theoretical calculations (Itikawa and Mason, 2005). A key question, however, is establishing the completeness and accuracy of the resulting cross-section sets, and it is here that experimental swarm physics continues to play an important role (Huxley and Crompton, 1974; Petrovic et al., 2009). The reader is referred to recent studies of electron swarms in water (Robson et al., 2011; Ness et al., 2012), where the consistency of electron–water cross-section sets with experimental swarm data has been investigated. The ability of swarm experiments to discriminate on the consistency or otherwise of the cross-section sets demands the most accurate transport theory to analyze the data. There is a large body of literature for swarm transport theory focussed on establishing such accuracy through benchmarking transport codes and simulations (Ness and Robson, 1986; Raspopović et al., 1999; Petrovic et al., 2002), including a recent study of positrons in water (Banković et al., 2012b). Our program aims to apply such theories and codes to the field of radiation damage modeling.

Often human tissue is simply treated as a gas at liquid densities in the field of radiation damage modeling, thus facilitating the use of the highly accurate gas-phase cross-sections that are available. Electron swarm measurements in liquids and dense gases generally indicate that such an assumption is questionable, however, particularly at low energies. We have recently developed a theory that combines the binary collision (gas-phase) cross-section data with information on the structural properties of the soft-condensed matter, thus allowing us to consider multiple (coherent) scattering effects (White and Robson, 2009, 2011). We believe that experimental swarm studies in liquids and dense gases provide key benchmarks required for accurately accounting for the soft-condensed nature of media in any transport theory or simulation used in modeling charged particle thermalization in human tissue. We explore this procedure further in this paper.

In this paper, we present the current status of our program of modeling low-energy electron and positron transport in water. In Section 2 we present two independent techniques for transport modeling—Boltzmann equation and Monte-Carlo simulation treatments. The key role of swarm physics in establishing the accuracy and consistency of cross-section sets is considered in Section 3 along with a discussion of the differences between electron and positron transport in water vapor and the differences between gas and liquid phase transport. We finish with a study of the thermalization of low-energy positrons (<150 eV) in water in Section 4.

2. Transport models: Boltzmann equation and Monte-Carlo simulation techniques

The analysis of charged particle motion in matter can be treated semi-classically by Boltzmann equation or Monte-Carlo simulation techniques. Both effectively follow an ensemble of particles as they move through phase-space (combined configuration $\boldsymbol{r}$ and velocity $\boldsymbol{c}$ spaces) under the action of forces and collisional processes. Boltzmann equation methods solve directly for the phase-space distribution function $f(\boldsymbol{r},\boldsymbol{c},t)$ (Boltzmann, 1872)

$$\frac{\partial f}{\partial t}+\boldsymbol{c}\cdot\nabla f+\frac{qE}{m}\cdot\frac{\partial f}{\partial \boldsymbol{c}}=-J(f). \tag{1}$$

Here $\boldsymbol{r}$ $\boldsymbol{c}$ denotes, the electric field while q and m are the charge and mass of the particle, respectively. Also, $J=J_{elas}+J_{inel}+J_{Ps}+J_a+J_{ion}$ is a linear collision operator representing the various collisional processes with the medium. The collision operator J_{elas} describes elastic scattering processes and the operator describing Ps formation, $J_{Ps}=n_0 c\sigma_{Ps}(c)$, where n_0 is the number density of the molecules of the background medium, and $\sigma_{Ps}(c)$ is the Ps formation cross-section. The positron annihilation operator J_a is similarly defined in terms of an annihilation cross-section $\sigma_a(c)$, while J_{inel} is taken here to be the semi-classical inelastic collision operator (Wang-Chang et al., 1964). For ionization processes, we implement the ionization collision operator J_{ion} detailed in Ness and Robson (1986). This is the microscopic picture. Solution for the phase-space distribution function $f(\boldsymbol{r},\boldsymbol{c},t)$ enables calculation of macroscopic measurable quantities through appropriate averages, e.g. the local charged particle density at time t is given by

$$n(\boldsymbol{r},t)=\int f(\boldsymbol{r},\boldsymbol{c},t)\,d\boldsymbol{c}. \tag{2}$$

Monte-Carlo simulation methods follow event by event the trajectory of each charged particle in the system. By considering an ensemble of such charged particles, one can then approximate (simulate) the charged-particle phase-space distribution function. Measurable macroscopic quantities are formed from appropriate averaging over the members of the ensemble.

In what follows, we briefly discuss the methods of solution and simulation used in this study. These independent techniques have been exhaustively tested against each other and against experiments for various benchmark systems. This is necessary to ensure the validity of the techniques.

2.1. Boltzmann equation treatment—a "multi-term" solution

Solution of the Boltzmann equation (1) requires decomposition of $f(\boldsymbol{r},\boldsymbol{c},t)$ in velocity space as discussed below. The first step in any analysis is typically the representation of the distribution function in terms of the directions of velocity space through an expansion in spherical harmonics (Robson and Ness, 1986)

$$f(\boldsymbol{r},\boldsymbol{c},t)=\sum_{l=0}^{\infty}\sum_{m=-l}^{l} f_m^{(l)}(\boldsymbol{r},c,t)Y_m^{[l]}(\hat{\boldsymbol{c}}), \tag{3}$$

where $Y_m^{[l]}(\hat{\boldsymbol{c}})$ are spherical harmonics and $\hat{\boldsymbol{c}}$ denotes the angles of $\boldsymbol{c}$. While common practice is to set the upper bound of the l-summation to 1 (i.e., the two-term approximation) and consider only $m=0$ (i.e., a Legendre polynomial expansion), we do not make any such restrictive assumptions in this theory, thus avoiding serious error (Ness and Robson, 1986; White et al., 2002). In best practice, the integer $l_{\max}$ is successively incremented until a prescribed accuracy criterion is met, as considered below. Combining (1) and (3) leads to the following hierarchy of coupled integro-differential equations for $f_m^{(l)}$:

$$\partial_t f_m^{(l)}+\sum_{l'm'}\left\langle lm\left|\boldsymbol{c}\cdot\nabla+\frac{e\boldsymbol{E}}{m}\cdot\frac{\partial}{\partial\boldsymbol{c}}\right|l'm'\right\rangle f_{m'}^{(l')}=-\sum_{l'm'}\langle lm|J|l'm'\rangle f_{m'}^{(l')}. \tag{4}$$

Expressions for the matrix elements of the streaming operator on the LHS are given in Robson and Ness (1986) and Ness and Robson (1986). The collision matrices e.g. $\langle lm|J|\,l'm'\rangle=[J_{elas}^{l}+J_{inel}^{l}+J_{Ps}^{l}+J_a^{l}+J_{ion}^{l}]\delta_{l',l}\,\delta_{m',m}$ are all diagonal in l and m, since the collision operators are all scalars. Details of the numerical schemes required for the solution of (4) are presented in the Appendix.

2.2. Monte-Carlo simulation technique

The Monte-Carlo simulation technique employed in swarm studies of the type considered below has been detailed and exhaustively benchmarked under a variety of field conditions and configurations, and we refer the reader to Petrovic et al. (2002), Dujko et al. (2008), and Raspopović et al. (1999) for details. For the field free space–time thermalization of positrons given in Section 4, we employ an independent code that operates in a manner similar to those described above. A positron/electron is generated, with a velocity sampled from some initial distribution. It then undergoes a series of collisions with water molecules, transferring energy and momentum at each collision as determined by the appropriate cross-section set. At pre-set time intervals and at each collision, a number of properties are sampled for each positron/electron, and these properties are later combined and analyzed to produce the outputs described in Section 2.3.

Between collisions, each positron has a free flight time determined from the (energy-dependent) collision frequency

$$t_F = \frac{-\log(R)}{\nu(\epsilon)}, \tag{5}$$

where R is a uniform pseudo-random number selected on the range [0,1), and $\nu(\epsilon)$ is the total collision frequency, which for a cold medium is given by

$$\nu(\epsilon) = n_0\sqrt{\frac{2\epsilon}{m}}\sigma_T(\epsilon). \tag{6}$$

Here $\sigma_T(\epsilon)$ represents the collision energy-dependent total electron/positron–molecule cross-section. The movement of the positron is simulated for the time period t_F, which, in the absence of electric fields and collisions, is a linear translation through space. At the end of that time period, the positron undergoes a collision with a water molecule which is generated at that position. The simulations reported in this paper are in a cold medium, so the molecule velocity contribution to the center of mass collision energy is neglected. The collision mechanics are performed in the center-of-mass frame, and the angular deflections are performed by transforming into a rotated co-ordinate system where the relative velocity is along the z-axis. A collisional process is chosen from the available collisional processes (elastic, direct ionization, etc.) by taking a cumulative sum of their respective probabilities, and mapping it onto a random variant on the range [0,1). The process threshold energy is deducted from the positron's energy, and this is used to scale the velocity that results from the angular transform. The scattering angle is determined from the differential cross-section. The system is rotated to reverse the initial rotation, and then the positron's lab frame velocity is calculated. This procedure is repeated until a pre-set ending condition is reached, and then repeated for a pre-set number of particles, after which the simulation is stopped and all results saved.

With most Monte-Carlo simulations, the error on each statistical quantity is proportional to the inverse of the square-root of the number of particles simulated, so there is no theoretical limit to the precision that may be achieved. In practice, performing the simulation takes a time proportional to the number of particles, so any way of increasing the rate of convergence is desirable. A large body of work exists in the literature concerning 'variance reduction' techniques, which are methods of ensuring that the particles that are simulated are the particles that have the most statistical significance, whilst still remaining representative of the system. One such technique that has proven useful in this simulation is a procedure that allows positrons to continue contributing to the statistics even after they have undergone an attachment process such as positronium formation. Every time a positron undergoes a collision, the probability of it forming positronium is discounted, forcing it to undergo another process. However, the positron is assigned a weight according to the probability that it has not formed positronium, and all summed statistics become a weighted sum that takes into account the positron's probability of existence. This allows the simulation to account for low-probability behavior that would otherwise be masked by the positronium formation, leading to increased detail that could only otherwise be achieved by simulating infeasibly large numbers of particles. Benchmarks have been performed to confirm that this technique is statistically accurate and does not introduce any bias into the results.

The majority of the code is written in Python, with a highly optimized Fortran kernel that performs the simulation work. The kernel is recompiled for each set of inputs, with most parameters hard-coded using a Python template language to insert them directly into the kernel's source code. This allows for a number of compile-time optimizations, whilst retaining a great deal of flexibility. In addition, all the probability calculations are implemented with direct lookup tables, and sampling uses dedicated, optimized algorithms for each variety of sample mesh. Because each positron can be simulated independently, this type of simulation lends itself very well to parallel and batch execution. This is exploited by the Python management code, which can schedule any number of independent simulations across any number of target processing units, and then later combine the results.

2.3. Measurables: transport coefficients and properties

2.3.1. General properties

The space–time evolution of a measurable property of the system $\psi(\boldsymbol{c})$ (e.g. flux $n\boldsymbol{c}$, or energy $\frac{1}{2}mc^2$ is calculated from the phase-space distribution function via an appropriate integral over all velocities

$$\langle\psi\rangle(\boldsymbol{r},t) = \frac{1}{n}\int \psi(\boldsymbol{c})f(\boldsymbol{r},\boldsymbol{c},t)\,d\boldsymbol{c}. \tag{7}$$

Global properties (e.g. total number of particles or collisions) are calculable through averages of the entire phase-space

$$\langle\langle\psi\rangle\rangle = \frac{1}{N}\int\int \psi(\boldsymbol{c})f(\boldsymbol{r},\boldsymbol{c},t)\,d\boldsymbol{c}\,d\boldsymbol{r}, \tag{8}$$

where N is the total number of particles

$$N = \int n(\boldsymbol{r},t)\,d\boldsymbol{r} = \int\int f(\boldsymbol{r},\boldsymbol{c},t)\,d\boldsymbol{c}\,d\boldsymbol{r}. \tag{9}$$

For Monte-Carlo simulations, these quantities are calculated through the appropriate averages of the ensemble of particles in the simulation (Dujko et al., 2006; Kumar et al., 1980; Raspopović et al., 1999).

2.3.2. Transport coefficients in swarm experiments

Experimental swarm investigations of transport behavior are generally made by sampling charged particle currents or densities $n(\boldsymbol{r},t)$. The connection between experiment and theory is made through the equation of continuity

$$\frac{\partial n(\boldsymbol{r},t)}{\partial t} + \nabla\cdot\boldsymbol{\Gamma}(\boldsymbol{r},t) = S(\boldsymbol{r},t), \tag{10}$$

where $\boldsymbol{\Gamma}(\boldsymbol{r},t) = n\langle\boldsymbol{c}\rangle$ is the positron flux and $S(\boldsymbol{r},t)$ represents the production rate per unit volume per unit time arising from non-conservative collisional processes such as Ps formation or annihilation for positron systems, or ionization and attachment processes for electrons. In the *hydrodynamic regime*, the space–time dependence is projected onto functionals of the number density through a density gradient relation (see e.g. the functional relationship (18) in Appendix), and so the flux $\boldsymbol{\Gamma}(\boldsymbol{r},t)$ and source

term $\boldsymbol{S}(\boldsymbol{r},t)$ in (10) are expanded as follows:

$$\boldsymbol{\Gamma}(\boldsymbol{r},t) = \boldsymbol{W}_F n(\boldsymbol{r},t) - \mathbf{D}_F \cdot \nabla n(\boldsymbol{r},t) + \cdots, \tag{11}$$

$$\boldsymbol{S}(\boldsymbol{r},t) = S^{(0)} - \boldsymbol{S}^{(1)} \odot \nabla n(\boldsymbol{r},t) + \mathbf{S}^{(2)} \odot \nabla\nabla n(\boldsymbol{r},t) + \cdots, \tag{12}$$

where $\boldsymbol{W}_F$ is the *flux* drift velocity and $\mathbf{D}_F$ is the *flux* diffusion tensor. Substitution of expansions (11) and (12) into the continuity Eq. (10) yields the diffusion equation

$$\frac{\partial n}{\partial t} + \boldsymbol{W} \cdot \nabla n - \mathbf{D} : \nabla\nabla n + \cdots = -R_a n, \tag{13}$$

where $R_a = -S^{(0)}$ is the loss-rate and we define the *bulk* transport coefficients

$$\boldsymbol{W} = \boldsymbol{W}_F + S^{(1)}, \tag{14}$$

$$\mathbf{D} = \mathbf{D}_F + S^{(2)}. \tag{15}$$

Swarm experiments are generally analyzed on the basis of the diffusion equation and hence the bulk coefficients, not the flux, are generally determined in swarm experiments (Robson et al., 2005). See Appendix for details of calculating the transport coefficients from the phase-space distribution function and from Monte-Carlo simulations.

3. Swarm experiments and studies

3.1. Swarms—a test of the completeness and accuracy of cross-section sets, and benchmarks for simulations

Modeling of macroscopic systems requires the availability of complete elastic, rotation, vibration, ..., cross-sections. While theoretical and experimental, e.g. crossed-beam, trap-based beam techniques (Surko et al., 2005) provide accurate individual cross-sections, they are often over a restricted energy range, and one must compile the complete set of available cross-section sets by extrapolating/interpolating over the necessary energy ranges. Their completeness and accuracy may then be assessed by swarm experiments. Here charged particles (e.g. electrons, positrons, etc.) are released into a medium (e.g. gas, liquid, etc.) and move under the action of applied electric and magnetic fields. The charged particles drift and diffuse down the drift tube under carefully controlled conditions (e.g. space-charge effects are minimized, field distributions are uniform, boundary effects are minimized). The resulting currents are then interpreted in terms of transport coefficients such as drift velocity (mobility) and diffusion coefficients. Such experiments are distinctly different from beam experiments: (i) they are multi-scattering experiments, and (ii) the velocity distribution function is not prescribed, and is often significantly non-Maxwellian by virtue of the electric field driving the charged particles out of thermal equilibrium. The connection between the microscopic cross-section and the macroscopic transport properties is provided by the Boltzmann equation and/or Monte-Carlo simulation. The cross-section sets are input into these transport theories/simulations and transport properties are then derived from them as discussed above. Correspondence of measured and calculated transport coefficients provides a test for the completeness and accuracy of the cross-section set. By varying the reduced electric field E/n_0, one can selectively sample the various energy regions and hence sample the completeness and accuracy of the cross-sections over the desired energy range. The reader is referred to Huxley and Crompton (1974) and Petrovic et al. (2009) for a complete discussion of electron swarm experiments, swarm data and analysis, and the recent reviews for positron swarms (Charlton, 2009) and electron swarms in dense gases and liquids (Sakai, 2007; Borghesani, 2006).

3.2. Electron and positron swarms in water vapor

Low-energy electrons liberated from primary radiation are produced in copious quantities ($\sim$ 40,000 per MeV of primary radiation). These low-energy electrons have been demonstrated to play an important role in radiation damage (Boudaiffa et al., 2000) and hence accurate models of electron transport in human tissue are required to understand and predict the associated damage caused. Positron-based medical imaging technologies (PET) and therapies, as well as indirect measurements of ion-beam dose arising from positron emitting fragments, demand an understanding of positron transport in modeling of electron and positron transport in biological matter. This requires the development of a complete and accurate cross-section set for electrons and positrons (Banković et al., 2012b) in water as a surrogate for human tissue.

Recently, we have been involved in the assessment of cross-section sets for electrons in water vapor (Robson et al., 2011; Ness et al., 2012) using swarm techniques. This has involved reconciling differences in definitions of drift velocity coefficients arising from theoretical and recent swarm experimental techniques (Robson et al., 2011; Hasegawa et al., 2007; Elford, 1995; Ruíz-Vargas et al., 2010). We have also assessed the accuracy and consistency of a recently recommended cross-section set (Itikawa and Mason, 2005) as well as recently obtained rotational, vibrational and electronic excitation cross-sections (Ness et al., 2012).

In Fig. 1, we compare the experimental drift velocities with those calculated using what we believe is the current best set of electron–water cross-sections (Ness et al., 2012). We also highlight in this figure the differences in the bulk and flux transport coefficients that arise from non-conservative collisional processes (attachment and ionization). For example, at around 100 Td, the bulk and flux drift velocities begin to diverge due to significant ionization. The bulk drift velocity is greater than the flux drift velocity due to the enhancement of the center of mass brought about by preferential ionization at the front of the swarm, where electrons on average have the highest energy.

A cross-section set for positrons in water vapor has recently been proposed based on currently available measured and theoretical cross-sections (Banković et al., 2012a). Currently, there is no

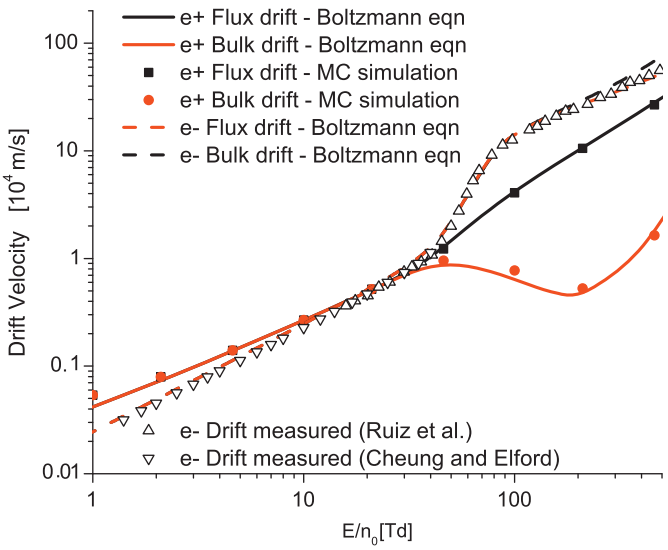

Fig. 1. Comparison of electric field dependence of the electron and positron drift velocities in water vapor. The line profiles are Boltzmann equation calculations while the solid symbols denote values from the Monte-Carlo simulation. The open symbols are experimental measurements (Ruíz-Vargas et al., 2010; Cheung and Elford, 1990).

experimental swarm transport data for positrons in water vapor to assess the completeness and accuracy of the set. It is illustrative, however, to utilize the proposed cross-section set to identify how differences in the microscopic cross-sections manifest themselves in macroscopic transport properties (Banković et al., 2012a; White et al., 2012). This will allow us to assess the validity of using electron cross-sections too model positron transport, as well as provide motivation for the future development of positron swarm experiments. The results are displayed in Fig. 1. One of the key channels open in positron scattering is the non-conservative process of Ps-formation. This channel is very strong from around the threshold at 5.8 eV to 20–30 eV. The manifestation of Ps-formation is highlighted in the differences between the bulk and flux drift velocities. We see that the differences appear at lower reduced fields than for electrons, reflecting the lower threshold energy of Ps than for electron-impact ionization. In contrast to the electron case, the bulk drift velocity is now reduced compared with the flux. Here positrons are preferentially lost from the front of the swarm through Ps-formation, which acts to shift the center-of-mass in a direction opposite to the field force direction. Strikingly, the strength of the Ps-formation process is such that the bulk drift velocity exhibits negative differential conductivity (NDC) i.e. a reduction in the bulk drift velocity with increasing electric field. NDC has been predicted in most positron systems (Bankovic et al., 2009; Banković et al., 2012b) and has been observed experimentally (Böse et al., 1981).

3.3. Swarm experiments in the dense gas and liquid phases

As discussed in Section 1, a key question in improving models of electron and positron transport in human tissue is how to account correctly for the soft-condensed nature of the medium, i.e. the existence of (short-range) correlations in the material. Commonly, one assumes an effective gas-phase, whereby the soft-condensed medium is replaced by a gas scaled to the liquid density, and single scattering cross-sections are used in the simulation, without accounting for structure. This assumption can be in quantitative, and even qualitative error, particularly at low energies where such "multiple-scattering" effects are important (see e.g. Borghesani, 2006; Sakai, 2007). Thus electron swarms in liquid and dense gases provide key benchmarks that should be met by all theories and simulations used in the modeling of radiation damage. Various theories exist for electrons in non-polar liquids with the heuristic model of Borghesani and co-workers (Borghesani, 2006) and Atrazhev and co-workers (Atrazhev and Dmitriev, 1986) of particular note. Theoretical models for electrons in polar liquids are limited (Polischuk, 1985), due in part to the lack of experimental data for such systems.

As detailed above, due to the density of liquid water, there exists many "multiple-scattering" effects that should be accounted for in a transport model for such systems (Borghesani, 2006; Sakai, 2007). The relevant length scales where these effects become important relate to the de Broglie wavelength of the electron/positron, the mean free path and the inter-particle spacing. Perhaps the most important consideration is when the de Broglie wavelength is greater than or comparable to the inter-particle spacing, resulting in the existence of coherent scattering from spatially and temporally correlated scattering centers in the medium. Recently, we have developed a generalized transport theory which accurately accounts for such processes (White and Robson, 2009, 2011). The theory utilizes only measurable quantities as inputs: (i) single-particle gas-phase cross-sections $\sigma(c,\chi)$ where χ is the scattering angle, and (ii) a static structure factor $S(\Delta k)$. This results in a structure-modified cross-section $\Sigma(c,\chi)=S(\Delta k)\sigma(c,\chi)$ used to describe momentum transfer (and higher) processes necessarily accounting for both configurational and kinetic phenomena present in transport of liquids and soft-condensed matter. In general, coherent scattering effects tend to reduce the momentum transfer cross-section for the process. In the limit where correlations do not exist, the theory reduces to the traditional gas-phase kinetic equation as required.

In Fig. 2, we highlight the impact of liquid structure effects on the drift velocity of positrons in water. Results for liquid water are compared with those under a gas-phase assumption (i.e. gas-phase cross-sections only) at liquid densities. We have implemented the cross-section set detailed in Banković et al. (2012b) with liquid structure effects accounted for through the static structure factor measured in Badyal et al. (2000). Differences between two sets of results occur only in the region where the de Broglie wavelength of the positron becomes comparable or greater than the average inter-particle spacing, and coherent scattering effects become important. At high fields (and hence high energies), the de Broglie wavelength is sufficiently small that the coherent effects are absent and liquid and gas phase results merge. This is consistent with experimental results for electrons. Coherent scattering reduces the momentum transfer, and thus enhances the positron drift velocity in the liquid phase as compared with that in the gas phase, as shown in Fig. 2. This behavior is also consistent with experimental results for electrons.

This represents a first step in going beyond the gas-phase assumption, but there are a variety of other multiple-scattering effects that need to be included. Limited experimental studies of electrons in dipole liquids indicate the possibility of localized and delocalized states for electrons. We have recently developed a new transport theory that accounts for such effects (Robson et al., in preparation).

4. Low-energy positron thermalization in water

In this section, we change our focus from the previous study of hydrodynamic swarms to consider non-hydrodynamic temporal and spatial relaxation of positrons in water vapor. We must emphasize, however, that the transport codes used to treat these systems are identical, and have been exhaustively benchmarked under hydrodynamic conditions. In this work, we restrict our study to the thermalization of low-energy positrons (<150 eV) to be consistent with the cross-section set detailed in Banković et al. (2012b) and implemented in this work. In what follows, we assess the impact of cross-sections and assumptions on the collisional

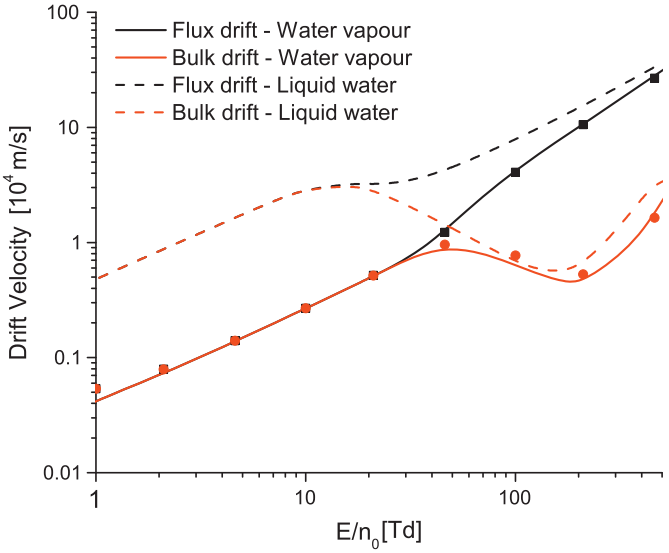

Fig. 2. Comparison of positron drift velocities in water using the gas-phase assumption with those accounting for liquid structure through coherent scattering effects.

dynamics on the spatio-temporal thermalization of positrons in water vapor.

In Fig. 3 we present a Monte-Carlo simulation of the event-by-event temporal relaxation of a sample of 50 positrons as they thermalize in water vapor at liquid water densities from 150 eV. The figure highlights the energy of the positron and the type of collisional process as a function of time. We observe that the various collision types are often clusters at various times, reflecting the energy dependence of the cross-section as the positrons thermalize.

Next, we consider the space–time evolution of the Ps-formation rate for a beam of 150 eV positron injected into water vapor at liquid densities. Rather than spatial track structures, we consider the measurable macroscopic quantities, which are averages over the tracks. Approximately 10^5 positrons have been simulated and the average over these tracks yield the per-particle spatio-temporal Ps-formation rate displayed in Fig. 4. If integrated over all times we can obtain the steady-state spatial Ps-formation rates. The rate has a peak value slightly over an Angstrom from the source, giving us an indication of the average positron range (i.e. average distance between the source of positrons and the point where the gamma-rays are emitted, a quantity of interest in PET modeling). There is a wealth of other information present in Fig. 4. The linear region contains those positrons that have not undergone collisions, maintaining their initial energy of 150 eV, and who are thus strong candidates for an ionization event and subsequent formation of Ps. Those positrons below the linear regime have undergone energy exchange collisions, decreasing their speed and in many cases changing their direction of travel, reducing their distance from the source. Since the peak in the Ps-formation cross-section occurs at approximately 20 eV, the peak in the Ps-formation rate consequently occurs below the line on the space–time plot. As the positrons continue to thermalize at longer times, their energy falls below the threshold for Ps-formation and the rate consequently decreases.

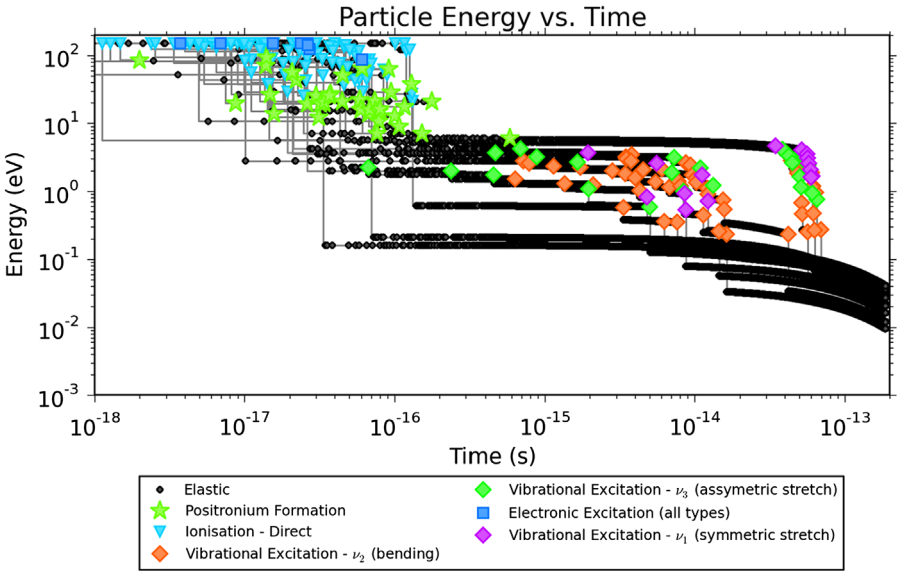

Fig. 3. Temporal variation of the collisional energy deposition for a 150 eV positron beam in water vapor at a liquid density.

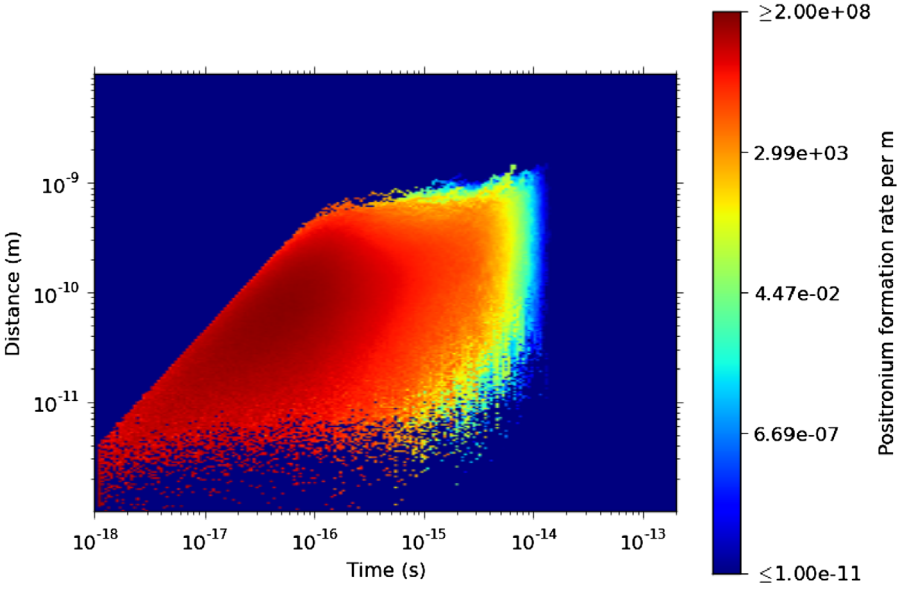

Fig. 4. Space–time variation of the positronium formation rate for a 150 eV beam of positrons in water vapor at liquid density. All collisions are assumed isotropic. Energy partitioning between the electron and positron in ionization events is assumed uniform.

In Fig. 5, we consider the explicit effects of anisotropy in the differential elastic cross-section. We implement the differential elastic cross-sections detailed in Baluja et al. (2007). The strongly forward peaked nature of the elastic cross-section for positrons in water vapor is reflected in the space–time Ps-formation evolution. The distance from the source to the peak in the Ps-formation rate is increased. In addition, the spread in the contours at low energies is reduced, indicative of the lack of transverse elastic scattering which tends to broaden the spectrum of positron energies at any given distance. We should note that all other scattering processes have been assumed isotropic.

In Fig. 6, we highlight the effects associated with the post-collision energy sharing in positron-impact ionization. In Fig. 4, the post-collision energy is assumed to be uniformly distributed between the scattered positron and the ejected electron (i.e. all fractions are equiprobable). We compare that with Fig. 6 in which we assume all energy resides with the scattered positron. The actual distribution of energies between the two post-collision particles varies with the incident positron energy (Charlton, 1985). The contour profiles are significantly altered under this assumption. The positrons tend to have a higher average energy at any given time since the post-collision energy is no longer shared. This shifts the peak in the Ps-formation to larger distances and longer times, but it also increases the overall rate of Ps-formation since the ionization process is much less likely to drop the positron's energy to below the Ps-formation threshold.

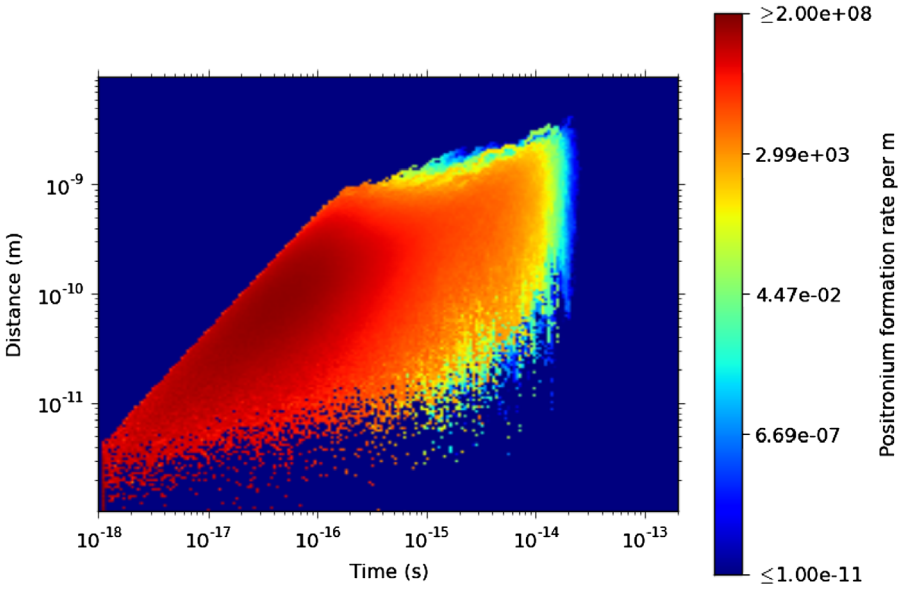

Fig. 5. Impact of the anisotropic nature of elastic scattering on the space–time variation of the positronium formation rate for a 150 eV beam of positrons in water vapor at liquid density. Anisotropic elastic collisions using the differential cross-sections of Baluja et al. (2007) are implemented. All other collision processes are assumed isotropic. Energy partitioning between the electron and positron in ionization events is assumed uniform.

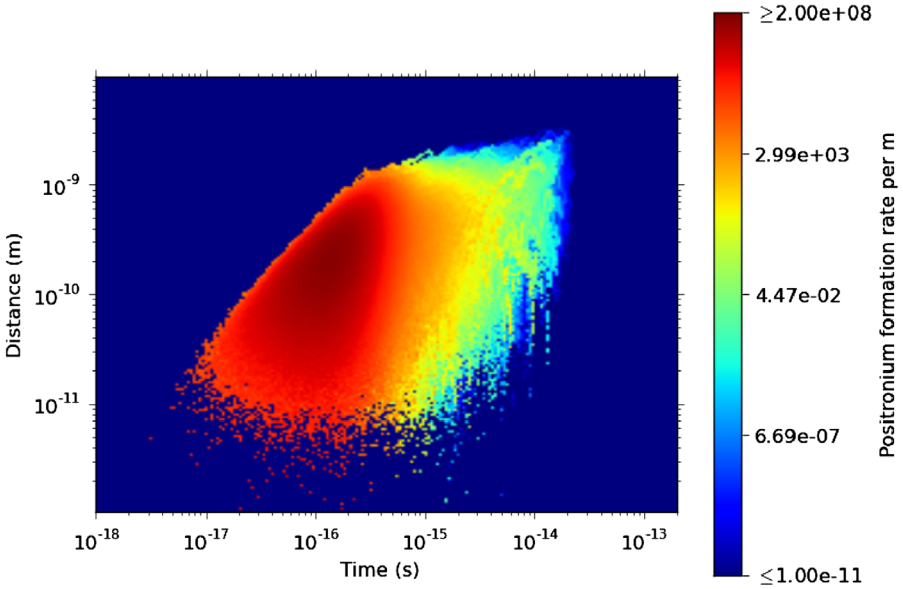

Fig. 6. Impact of the nature of post-collision energy sharing between the ejected electron and the scattered positron in an ionization process on the space–time variation of the positronium formation rate for a 150 eV beam of positrons in water vapor at liquid density. All collision processes are assumed isotropic. All post-collision energy is given to the scattered positron in ionization collision processes.

5. Concluding remarks

This paper highlights recent developments in the modeling of low-energy (<150 eV) electron and positron transport in biological systems, with a particular focus on water using the recently proposed cross-section set for this energy region (Banković et al., 2012b). We have demonstrated and emphasized the important role of swarm physics in assessing the accuracy and completeness of cross-section sets required for such modeling. Such swarm experiments are currently not available for positrons, and we hope that our studies will provide motivation for the development of new positron swarm experiments and extension of existing electron swarm experiments to consider biological targets. We have also highlighted the importance of benchmarking Monte-Carlo simulation and other transport codes used in this modeling, and here again swarms can play an important role. A first step in overcoming the 'gas-phase assumption' was presented by including explicitly the temporal and spatial correlations that exist in liquids through a modification of the gas-phase cross-sections via the static structure factor to account for coherent scattering effects. We have provided evidence that these effects need to be clearly included in any study of low-energy electron/positron transport in biological material. While the current manuscript focussed on low-energy processes less than 150 eV, the aim is to extend these electron and positron cross-section sets to higher energies and facilitate an accurate simulation of positron and secondary electron transport in PET and positherapy. Furthermore, we will combine the water cross-section set with recent measurements/calculation of cross-sections for various biomolecules to provide a more realistic representation of biological matter.

Acknowledgments

We thank the Australian Research Council through its Centers of Excellence and Discovery programmes for financial support, the Australian Academy of Science through its European Scientific Exchange Program and Nano-IBCT COST Action. S.D., Z.Lj.P. and A.B. were supported by MNRS Projects ON171037 and III41011 G.G. was partially supported by the Spanish Ministerio de Economia e Innovacion (Project FIS2009-10245).

Appendix A. Boltzmann equation solution—speed and spatial representations

Further numerical treatment is required to solve the system of equations detailed in (4). Various numerical techniques are suitable for representing the speed/energy space (Robson and Ness, 1986; Mason and McDaniel, 1988) in the multi-term representation (3). In this paper, we employ an expansion in terms of generalized Sonine (generalized Laguerre) $R_{vl}(\alpha c)$ polynomials (Chapman and Cowling, 1939)

$$f_m^{(l)}(\boldsymbol{r},c,t) = w(\alpha,c)\sum_{v=0}^{\infty} F_\alpha(vlm;\boldsymbol{r},t)R_{vl}(\alpha c), \tag{16}$$

which are orthonormal with respect to a Maxwellian weight function

$$w(\alpha,c) = \left(\frac{\alpha^2}{2\pi}\right)^{3/2}\exp\left\{\frac{-\alpha^2 c^2}{2}\right\},$$

where $\alpha^2 = m/kT_b$. The parameter T_b is chosen to be an arbitrary basis temperature and is traditionally referred to as the 'two-temperature theory' (Lin et al., 1979; Ness and Robson, 1986).

Substituting (3) and (16) into (1), and utilizing the orthonormality of the basis functions, we obtain the following infinite set of partial differential equations for the moments $F_\alpha(vlm;\boldsymbol{r},t)$

$$\sum_{v'=0}^{\infty}\sum_{l'=0}^{\infty}\sum_{m'=-l'}^{l'}\left[\langle vlm\left|J+\frac{q\boldsymbol{E}}{m}\cdot\frac{\partial}{\partial\boldsymbol{c}}+\boldsymbol{c}\cdot\nabla\right|v'l'm'\rangle\right]F_\alpha(vlm)=0, \tag{17}$$

where

$$\langle vlm|\,|J+\frac{q\boldsymbol{E}}{m}\cdot\frac{\partial}{\partial\boldsymbol{c}}+\boldsymbol{c}\cdot\nabla|\,|v'l'm'\rangle$$

are matrix elements of the collision and streaming operators (Ness and Robson, 1986).

In the hydrodynamic regime, the space–time dependence of f is projected out through a density gradient expansion (Kumar et al., 1980; White et al., 2009)

$$f(\boldsymbol{r},\boldsymbol{c},t) = \sum_{k=0}^{\infty} f^{(k)}(\boldsymbol{c})\odot(-\nabla)^k n(\boldsymbol{r},t), \tag{18}$$

where $f^{(k)}(\boldsymbol{c},t)$ are tensors of rank k and $\odot$ denotes a k-fold scalar product. The convergence of this expansion was recently investigated (Dujko et al., 2008). Using spherical tensors, the expansion (18) takes the form (Robson and Ness, 1986)

$$F_\alpha(vlm)(\boldsymbol{r},t) = \sum_{s=0}^{2}\sum_{\lambda=0}^{s} F(vlm|s\lambda)G_m^{(s\lambda)}n(\boldsymbol{r},t), \tag{19}$$

where $G_m^{(s\lambda)}$ is the irreducible gradient tensor operator (Robson and Ness, 1986). Substitution of (19) into (4) and equating coefficients of $G_m^{(s\lambda)}n(\boldsymbol{r},t)$, we obtain the following hierarchy of kinetic equations:

$$\begin{aligned}\sum_{v'=0}^{\infty}\sum_{l'=0}^{\infty}&\Big[n_0 J^l_{vv'}(\alpha)\delta_{ll'} - R_a\delta_{vv'}\delta_{ll'} + i\frac{qE}{m}\alpha(l'm10|lm)\langle vl\|K^{[1]}\|v'l'\rangle\\ &-n_0 J^0_{0v'}(\alpha)F_\alpha(vl0|00)(1-\delta_{s0}\delta_{\lambda 0})\delta_{l'0}\delta_{m0}\Big]F_\alpha(v'lm|s\lambda)\\ &=\overline{X}(vlm|s\lambda;\alpha),(v,l)=0,1,2,\ldots,\infty,\quad |m|\le\min\{l,\lambda\},\\ s+\lambda&=\text{even},\end{aligned} \tag{20}$$

where R_a is the net loss rate of charged particles and is defined in (21) below. The RHS vectors for the required members of the hierarchy are given by Eqs. (16), (18) and (20) of Ness and Robson (1986). The reduced matrix elements of the velocity derivative $\langle vl\|K^{[1]}\|v'l'\rangle$ are given by (12a) of Ness and Robson (1986). The reduced matrix elements of the collision operator have the form $\langle vlm\|J\|v'l'm'\rangle = J^l_{vv'}(\alpha)\delta_{ll'}\delta_{mm'}$ due to the scalar nature of the operator, and the evaluation of the elements is detailed in the following section. The lowest member of the hierarchy is an eigenvalue equation.

The transport coefficients of interest in the present study are be related to the calculated moments via

$$R_a = n_0\sum_{v'=0}^{\infty} J^0_{0v'}(\alpha)F_\alpha(v'00|00), \tag{21}$$

$$W = \frac{i}{\alpha}F_\alpha(010|00) - in_0\sum_{v'=1}^{\infty} J^0_{0v'}(\alpha)F_\alpha(v'00|11), \tag{22}$$

$$D_L = -\frac{1}{\alpha}F_\alpha(010|11) - n_0\sum_{v'=1}^{\infty} J^0_{0v'}(\alpha)[F_\alpha(v'00|20) - \sqrt{2}F_\alpha(v'00|22)] \tag{23}$$

$$D_T = -\frac{1}{\alpha}F_\alpha(011|11) - n_0 \sum_{\nu'=1}^{\infty} J^0_{0\nu'}(\alpha)\left[F_\alpha(\nu'00|20) + \frac{1}{\sqrt{2}}F_\alpha(\nu'00|22)\right]. \quad (24)$$

We re-emphasize here that there are two distinct 'sets' of coefficients: bulk and flux (Robson et al., 2005; Robson, 1991; Tagashira et al., 1978). The drift velocity and diffusion coefficients defined above are bulk coefficients. The components involving summations constitute the explicit non-conservative components of the transport coefficients, while the remainder constitute the flux contribution.

References

Atrazhev, V.M., Dmitriev, E.G., 1986. Hot electrons in atomic non-polar liquids with molecular impurities. J. Phys. C: Solid State Phys. 19 (August (22)), 4329–4338.

Badyal, Y.S., Saboungi, M.-L., Price, D.L., Shastri, S.D., Haeffner, D.R., Soper, A.K., 2000. Electron distribution in water. J. Chem. Phys. 112 (21), 9206.

Baluja, K.L., Zhang, R., Franz, J., Tennyson, J., 2007. Low energy positron collisions with water: elastic and rotationally inelastic scattering. J. Phys. B: Atom. Mol. Opt. Phys. 40 (September (17)), 3515–3524.

Banković, A., Dujko, S., White, R.D., Buckman, S.J., Petrović, Z.L., 2012a. On approximations involved in the theory of positron transport in gases in electric and magnetic fields. Eur. Phys. J. D 66 (July (7)), 174.

Banković, A., Dujko, S., White, R.D., Marler, J.P., Buckman, S.J., Marjanović, S., Malović, G., García, G., Lj Petrović, Z., 2012b. Positron transport in water vapour. New J. Phys. 14 (March (3)), 035003.

Bankovic, A., Petrovic, Z.L., Robson, R.E., Marler, J.P., Dujko, S., Malovic, G., 2009. Negative differential conductivity of positrons in gases. Nucl. Instr. Methods Phys. Res. Sect. B 267 (2), 350.

Boltzmann, L., 1872. Wein. Ber. 66, 275.

Borghesani, A.F., 2006. Electron and ion transport in dense rare gases. IEEE Trans. Dielect. Elect. Insul. 13 (June (3)), 492–502.

Böse, N., Paul, D.A.L., Tsai, J.-S., 1981. Positron drift in molecular hydrogen. J. Phys. B: Atom. Mol. Phys. 14 (September (18)), 3535.

Boudaiffa, B., Cloutier, P., Hunting, D., Huels, M.A., Sanche, L., 2000. Resonant formation of DNA strand breaks by low-energy (3 to 20 eV) electrons. Science 287 (5458), 1658–1660.

Chapman, S., Cowling, T.G., 1939. The mathematical theory of non-uniform gases. Cambridge University Press, Cambridge.

Charlton, M., 1985. Experimental studies of positrons scattering in gases. Rep. Prog. Phys. 48 (June (6)), 737–793.

Charlton, M., 2009. Positron transport in gases. J. Phys.: Confer. Ser. 162, 012003, April.

Cherry, S.R., Sorensen, J.A., Phelps, M.E., 2003. Physics in Nuclear Medicine. Saunders.

Cheung, B., Elford, M.T., 1990. The drift velocity of electrons in water–vapor at low values of E/n. Aust. J. Phys. 43 (6), 755–763.

Dujko, S., White, R.D., Ness, K.F., Petrović, Z.L., Robson, R.E., 2006. Non-conservative electron transport in CF_4 in electric and magnetic fields crossedat arbitrary angles. J. Phys. D: Appl. Phys. 39, 4788.

Dujko, S., White, R.D., Petrović, Z.L., 2008. Monte Carlo studies of non-conservative electron transport in the steady-state Townsend experiment. J. Phys. D: Appl. Phys. 41 (24), 245205.

Elford, M., 1995. Gaseous Electronics and its Applications. KTS Scientific, Kluwer, p. 34.

Enghardt, W., Parodi, K., Crespo, P., Fiedler, F., Pawelke, J., Panisch, F., 2004. Dose quantification from in-beam positron emission tomography. Radiother. Oncol. 73(Suppl. 2(0)), S96–98. Carbon-Ion Therapy, Proceedings of the Heavy Charged Particles in Biology and Medicine.

Hasegawa, H., Date, H., Shimozuma, M., 2007. Electron swarm parameters in water vapour. J. Phys. D: Appl. Phys. 40 (8), 2495–2498.

Huxley, L.G.H., Crompton, R.W., 1974. The Drift and Diffusion of Electrons in Gases. Wiley, New York.

Itikawa, Y., Mason, N., 2005. Cross sections for electron collisions with water molecules. J. Phys. Chem. Refer. Data 34 (1), 1–22.

Kumar, K., Skullerud, H.R., Robson, R.E., 1980. Kinetic theory of charged particle swarms in neutral gases. Aust. J. Phys. 33, 343.

Lin, S.L., Robson, R.E., Mason, E.A., 1979. Moment theory of electron drift and diffusion in neutral gases in an electrostatic field. J. Chem. Phys. 71, 3483.

Mason, E.A., McDaniel, E.W., 1988. Transport Properties of Ions in Gases. Wiley, New York.

Ness, K.F., Robson, R.E., 1986. Velocity distribution function and transport coefficients of electrons in gases: spherical harmonic decomposition of the Boltzmann equation. Phys. Rev. A 34, 2185.

Ness, K.F., Robson, R.E., Brunger, M.J., White, R.D., 2012. Transport coefficients and cross sections for electrons in water vapour: comparison of cross section sets using an improved Boltzmann equation solution. J. Chem. Phys. 136 (2), 024318, January (14).

Petrovic, Z.L., Dujko, S., Maric, D., Malovic, G., Nikitovic, Z., Sasic, O., Jovanovic, J., Stojanovic, V., Radmilovic-Radenovic, M., 2009. Measurement and interpretation of swarm parameters and their application in plasma modelling. J. Phys. D: Appl. Phys. 42 (19), 194002.

Petrovic, Z.L., Raspopović, Z., Dujko, S., Makabe, T., 2002. Kinetic phenomena in electron transport in radio-frequency fields. Appl. Surf. Sci. 192 (May (1–4)), 1–25.

Polischuk, A.Y., 1985. Theory of electron mobility in moderately dense polar gases. J. Phys. B: Atom. Mol. Phys. 18, 829.

Raspopović, Z.M., Sakadžić, S., Bzenić, S.A., Petrović, Z.L., 1999. Benchmark calculations for Monte Carlo simulations of electron transport. IEEE Plasma Sci. 27, 1241.

Robson, R.E., Philippa, B.W., White, R.D., in preparation.

Robson, R.E., 1991. Transport phenomena in the presence of reactions: Definition and measurement of swarm transport coefficients. Aust. J. Phys. 44, 685.

Robson, R.E., Ness, K.F., 1986. Velocity distribution function and transport coefficients of electrons in gases 2: moment equations and applications. Phys. Rev. A 33 (March (3)), 2068.

Robson, R.E., White, R.D., Ness, K.F., 2011. Transport coefficients for electrons in water vapor: definition, measurement, and calculation. J. Chem. Phys. 134 (February (6)), 064319.

Robson, R.E., White, R.D., Petrović, Z.L., 2005. Physically based fluid modelling of collisionally dominated low-temperature plasmas. Rev. Mod. Phys. 77, 1303–1320.

Ruíz-Vargas, G., Yousfi, M., de Urquijo, J., 2010. Electron transport coefficients in the mixtures of H_2O with N_2, O_2, CO_2 and dry air for the optimization of non-thermal atmospheric pressure plasmas. J. Phys. D: Appl. Phys. 43 (November (45)), 455201.

Sakai, Y., 2007. Quasifree electron transport under electric field in nonpolar simple-structured condensed matters. J. Phys. D: Appl. Phys. 40 (December (24)), R441–R452.

Surko, C.M., Gribakin, G.F., Buckman, S.J., 2005. Low-energy positron interactions with atoms and molecules. J. Phys. B: Atom. Mol. Opt. Phys. 38, R57–R126.

Tagashira, H., Taniguchi, T., Kitamori, K., Sakai, Y., 1978. Development of electron avalanches parallel and perpendicular to the electric field-a Boltzmann equation analysis. J. Phys. D 11, L43.

Wang-Chang, C.S., Uhlenbeck, G.E., De Boer, J., 1964. In: Boer, J.D., Uhlenbeck, G.E. (Eds.), Studies in Statistical Mechanics, vol. II. Wiley, New York, p. 241.

White, R., Robson, R.E., Dujko, S., Nicoletopoulos, P., Li, B., 2009. Recent advances in the application of Boltzmann equation and fluid equation methods to charged particle transport in non-equilibrium plasmas. J. Phys. D: Appl. Phys. 42, 194001.

White, R., Sullivan, J., Bankovic, A., Dujko, S., Robson, R., Petrovic, Z.L., Gomez-Tejedor, G.G., Brunger, M., Buckman, S., 2012. Positron and electron interactions and transport in biological media. In: Garcia Gomez-Tejedor, G., Fuss, M.C. (Eds.), Radiation Damage in Biomolecular Systems. Biological and Medical Physics, Biomedical Engineering. Springer, The Netherlands, pp. 227–238.

White, R.D., Robson, R.E., 2009. Positron kinetics in soft condensed matter. Phys. Rev. Lett. 102 (23), 230602.

White, R.D., Robson, R.E., 2011. Multiterm solution of a generalized Boltzmann kinetic equation for electron and positron transport in structured and soft condensed matter. Phys. Rev. E 84 (September (3)), 1–10.

White, R.D., Robson, R.E., Schmidt, B., Morrison, M.A., 2002. Is the classical two-term approximation of electron kinetic theory satisfactory for swarms and plasmas? J. Phys. D: Appl. Phys. 36, 3125–3131.